

tFold-TR: Combining Deep Learning Enhanced Hybrid Potential Energy for Template-Based Modelling Structure Refinement

Liangzhen Zheng, Haidong Lan, Tao Shen, Jiaxiang Wu, Sheng Wang, Wei Liu, Junzhou Huang*

Tencent AI Lab, Shenzhen 518057, China

*Correspondence: Junzhou Huang
Email: joehhuang@tencent.com

Abstract

Proteins structure prediction has long been a grand challenge over the past 50 years, owing to its broad scientific and application interests. There are two major types of modelling algorithms, template-free modelling and template-based modelling. The latter one is suitable for easy prediction tasks and is widely adopted in computer-aided drug discoveries for drug design and screening. Although it has been several decades since its first edition, the current template-based modeling approach suffers from two important problems: 1) there are many missing regions in the template-query sequence alignment, and 2) the accuracy of the distance pairs from different regions of the template varies, and this information is not well introduced into the modeling. To solve the two problems, we propose a structural optimization process based on template modelling, introducing two neural network models to predict the distance information of the missing regions and the accuracy of the distance pairs of different regions in the template modeling structure. The predicted distances and residue pairwise-specific deviations are incorporated into the potential energy function for structural optimization, which significantly improves the qualities of the original template modelling decoys.

Author Summary

Protein structures are fundamental information for understanding protein functions and biological processes. While experimental protein structure determination methods are time-consuming and expensive, the protein structure prediction methods are faster and high-throughput, and they are of great value to obtain near-experimental structure predictions. Template-based modelling method, as one of the most commonly used and successful algorithms in the early days for structure prediction, is often used to generate homologous protein models for drug screening or functional analysis and has two major drawbacks. We focus on solving the problems in the template-based modelling method by complementing the missing template information predicted by a deep learning model and introducing more dynamic restraints by considering the template-based modelling local quality. The refinement protocol largely improves the template-based modelling results. This method may be further improved by incorporating a more accurate template-based modelling result quality assessment method, and it would benefit protein homology modelling, function analysis as well as drug designs.

1. Background

Proteins participate in almost all the important biological activities in different organisms, the structure information is vital to understand the protein functions. Since the 1960s, several experimental methods, such as X-ray spectroscopy^{1,2}, Nucleic Magnetic Resonance (NMR)³⁻⁵, small-angle X-ray scatter⁶⁻⁸, and Cryogenic Electron Microscopy (cryo-EM)⁹⁻¹², have been developed to determine protein structures. These experimental methods are not only time-consuming but also quite expensive, thus they restrict the high throughput applications for protein structure determination in biological sciences and the pharmaceutical industry. The conflict, as well as the accessibility of large-scale computational power, thus promotes the rise of computational methods for protein structure predictions.

Computer-aided protein structure prediction is based on a naive assumption: the structure of a protein is uniquely determined by its amino acid sequence¹³⁻¹⁵. The assumption then could be further extended to another one: proteins with similar sequences could share a common folding pattern. These assumptions, therefore, urge us to consider a protein structure prediction method based on sequence identical or similar proteins whose structures have been determined. Template-based modelling (TBM)¹⁶⁻²³ as the most pioneer protein structure prediction algorithm is developed.

Common TBM pipelines are composed of three major steps: template searching, template-query sequence alignment, and three-dimensional (3D) modelling. Firstly, by sequence similarity searching (BLAST^{24,25} or HHblits²⁶) among the sequences of structure determined proteins (in Protein Data Bank), a template (which has the highest sequence similarity score to the query protein sequence) is selected. Secondly, the template sequence is aligned with the query sequence to generate the template-query alignment, then the corresponding coordinates of backbone atoms (in the well-aligned region of the alignment) in the template protein structure thus are duplicated to serve as the initial coordinates for the aligned residues in the query protein for modelling, whereas the residues in the unaligned region in the alignment thus would be modelled randomly. Finally, the initial conformation of the query protein is then subjected to energy minimization²⁷⁻³⁰, or Monte Carlo (MC) simulation, or molecular dynamics (MD) simulations^{28,31,32}, or a combination of them, guided by a certain potential energy function^{33,34} ($E(\mathbb{R})$) (Equation 1), which contains the general molecular mechanics (MM)^{35,36} (such as Charmm force field³⁷⁻⁴⁰ and Rosetta Ref2015 energy function¹⁷) and distance/contact/orientation constraints⁴¹⁻⁴⁷. The constraints used for structure refinements are C β -C β (or C α -C α) inter-residue distance constraints as depicted by $g(d_{i,j})$ in Equation 1, L indicates the length of the query sequence, and i and j are the indices of the residues, \mathbb{R} represents the conformation of the query protein in three-dimensional (3D) space. Lastly, the collected conformations from 3D-modelling are ranked^{33,34,48,49} or clustered⁵⁰ to select the best predictions.

$$E(\mathbb{R}) = \sum_{i,j}^L g(d_{i,j}) + P(\mathbb{R}) \quad (1)$$

The most popular TBM pipelines nowadays, such as RosettaCM¹⁷, Modeller³³, SWISSMODEL^{40,51}, I-TASSER⁵²⁻⁵⁵, and RaptorX⁵⁶⁻⁵⁸, all adopt a more or less similar protein structure prediction solution as described above.

Another type of modelling method is template-free modelling (FM), or *de novo* prediction. Recently, more and more accurate deep learning models are applied in FM by providing an accurate residue-residue distances/orientations estimation^{41,42,59,60}. These distances are further utilized as the reference points for distance constraints in $g(d_{i,j})$ for minimization and refinement. In a 2019 paper⁴¹, Yang et al. proposed that orientations could also be adopted as structure constraints in Equation 1, and their work greatly lifts the overall FM accuracy.

However, in the current TBM pipelines, especially the single-template-based pipelines, the 3D modelling steps has two major problems. The first one is that for a query sequence, the best template often does not necessarily cover the entire query sequence. In one way, because different proteins have different lengths, even proteins of the same family may differ a lot in terminal regions or the loop regions. There could be regions in the query sequence without an aligned counterpart in the template sequence. In another way, in many X-ray experiments, the signals of some loops cannot be obtained, and there are defects in the PDB structure of the template, leading to missing reference coordinates for the query sequence. To deal with these two types of information missing, traditional single-template-based TBM pipelines adopted very naïve approaches by assuming no inter-residue distance constraints and leaving them rather mobile in the 3D modelling step. Although loop modelling methods have been developed to complete the loops, the accuracy is still to be improved^{33,61,62}. The second problem is that the current distance constraints of 3D modelling based on single-template are often treated equally^{16,17}. The accuracies of the distance pairs (extracted from the template structure) used for query protein modelling are not necessarily the same. Some regions in the template sequence are highly identical to the query sequence, the distances from these regions should be more credible, and some are less similar to the query sequence thus should be less reliable. For example, an accurate template can be found in the first half part of the query sequence, but the template similarity in the second half is relatively low. Intuitively, we should consider stronger inter-residue distance constraints for the first area and weaker distance constraints for the last half. At present, there have been some methods to estimate the strength of the distance constraint of the same position of multiple templates based on the variability of the distance of the same inter-residue distances^{63–66}. However, these methods assume that multiple templates can truly reflect the query residue-residue distance constraint distribution, which may not be true.

To solve the above two problems, we tried to 1) predict the inter-residue distances of all amino acids by a deep learning model to fill in the missing amino acid pair information, and 2) predict the inter-residue distance deviations of the template structure and the ground truth structure by another deep learning model to obtain the residue pairwise specific distance constraint strength. With the aid of the predicted distances and deviations, we design a hybrid potential equation that can better compensate for the shortcomings of the TBM pipelines. We call the whole structure optimization process Tencent Folding for Template-based Structure Refinement (tFold-TR) (Figure 1). Based on CASP13TBM and a CAMEO 3-month dataset, we optimized the TBM modeling decoys obtained by CNFpred's template selection and RosettaCM's 3D modelling and improved the modeling average accuracy GDT-TS from 66.8 to 74.8 and from 67.1 to 72.1, respectively. The refinement process also improves the accuracy of decoys generated by other threading and 3D modelling methods.

2. Results

2.1 Overall performance of tFold-TR

We compared the tFold-TR refinement performance of decoys generated by different TBM pipelines. For CASP13TBM dataset, we used three different threading methods (CNFpred, hhblit2, and BLAST) to identify the best template and used two different 3D modelling tools (Modeller and RosettaCM) to build the decoys of the query proteins based on a single-best-template. Among the 3 threading methods, CNFpred as a profile-profile threading method could provide the estimated best template for all the query sequences, whereas BLAST only predicts the templates for easy targets. As for the 3D modelling methods, with the same threading method, RosettaCM builds slightly better decoys when comparing to Modeller

(Figure 2). For example, the decoys generated by CNFpred+RosettaCM have an average GDT-TS = 66.0, whereas the average GDT-TS of decoys built by CNFpred+Modeller is 65.1. The same trend also goes for the other two threading methods on the other two datasets.

Starting from the TBM decoys generated by different threading-modelling combinations, the two strategies (*fixed-delta* and *predicted-delta*) implemented in tFold-TR further refine the results. On CASP13TBM dataset, when the templates are selected by CNFpred, and the decoys are comparative modelled by RosettaCM, the average accuracy (GDT-TS=66.0) is achieved. After the *fixed-delta* tFold-TR refinement, the average GDT-TS scores of the tFold-TR refined decoys raise to 72.9. Alternatively, the TBM decoys could be refined by *predicted-delta* tFold-TR, and the resulting average GDT-TS for the 74 proteins is 74.8. Thus, these results indicate that *predicted-delta* tFold-TR could increase the modelling accuracy by refining the TBM decoys. Interestingly, if we provided the ground true structures to derive the true distance deviation matrix for *delta* tFold-TR, the average GDT-TS of CASP13TBM dataset is 79.5, which serves as the upper boundary of the modelling accuracy without providing the ground truth inter-residue distance map. Similarly, if the TBM decoys are generated by CNFpred+Modeller, the average GDT-TS scores of the refined decoys by three refinement strategies (*fixed-delta*, *predicted-delta*, and *native-delta*) are 7.3, 9.5, and 15.3 higher than that of the initial models.

The refinement performance is also evaluated with the other two CAMEO datasets. For the CAMEO-HY dataset, *fixed-delta* and *predicted-delta* tFold-TR algorithms also increase the average GDT-TS from 65.1 to 69.2 and 72.8, when the initial models are modelled by CNFpred+RosettaCM. To assess the performance of tFold-TR, we collected all targets in CAMEO platform during 3 months period to form a relatively larger real-world dataset (CAMEO-3M) for evaluation. For this dataset, the average GDT-TS of initial TBM decoys (CNFpred+RosettaCM) is 67.1, and it is 70.2 and 72.1 after refinement by tFold-TR *fixed-delta* and *predicted-delta* strategies.

For all the 3 datasets, if we use different threading methods for template searching and different 3D modelling tool for decoy generate, tFold-TR pipeline could still refine the decoys and have similar accuracy improvements (Supplementary Table). To eliminate the bias from the evaluation metric (GDT-TS), TMscore and LDDT(global) scores are also calculated and the scores of tFold-TR are also higher than the initial models (Supplementary Table). In summary, tFold-TR pipeline could further refine the decoys generated by different TBM pipelines.

2.2 The comparison with other protein structure prediction method

We compared the performance of tFold-TR (CNFpred+RosCM with *predicted-delta* strategy) with other structure prediction methods. For the 3 datasets (Figure 2, D-F), tFold-TR shows the best performance (for both GDT-TS and LDDT score) than RaptorX^{42,43}, Zhang group^{67,68}, Robetta⁶⁹, and AlphaFold1^{59,60}.

On the CASP13TBM dataset, the decoys from Zhang group have the highest average GDT-TS score (71.97), and the decoys from AlphaFold1 have highest average global LDDT score (64.27). By applying refinement modelling using tFold-TR *predicted-delta*, the quality of the decoys generated by CNFpred+RosettaCM improves from GDT-TS 66.0, which is at the same level with BAKER team but lower than RaptorX-DeepModeller, to a higher score 74.75, much higher than all other groups mentioned above. The refined decoys by tFold-TR also have a higher average LDDT score (66.99). On a second dataset CAMEO-HY, we collected the modelling decoys from the other three servers (RaptorX, SwissModel, and Robetta). The initial models we adopted for tFold-TR refinement have much lower average GDT-TS = 65.1 than the three servers. However, after refinement, the quality of the decoys (average GDT-TS =

73.64) has been greatly enhanced and is the highest method among the solutions provided by the three servers and the TBM pipeline (CNFPred+RosettaCM).

Lastly, we also compared the performance of tFold-TR with other servers on the 3rd dataset CAMEO-3M. During the 3-month submission period, there several targets where no decoys were submitted by the 3 servers, so only the 171 commonly submitted protein targets were selected to make a fair comparison between different methods. SwissModel and Robetta generate better decoys, though SwissModel decoys have higher GDT-TS (71.64) scores whereas Robetta decoys have higher LDDT (70.49) scores. Our baseline TBM pipeline built the initial models for tFold-TR refinement on 171 targets, and the average GDT-TS score is increased from 67.1 to 72.2, and the average LDDT score is improved from XX to 69.23, which is slightly higher than Robetta.

Through the comparisons, it is obvious that the TBM pipeline (CNFPred+RosettaCM) is the least accurate method. Nevertheless, the TBM pipeline could be further improved by tFold-TR refinement protocol to generate much better decoys. And tFold-TR in combination with a TBM pipeline is one of the most accurate protein structure prediction methods.

2.3 The relationship between initial model quality and refinement performance

From the results obtained from CASP13TBM dataset (Figure 3A), the improvements of GDT-TS scores refined by tFold-TR (*predicted-delta* and *fixed-delta* strategy) are much more significant for medium to hard targets whose initial TBM model qualities are less than 60.0. A similar pattern is also found in CAMEO-HY dataset (Figure 3B) which contains mostly medium to hard targets. In contrast, for easy targets whose initial TBM decoy GDT-TS scores are higher than 80.0, the tFold-TR refinement could barely improve the TBM decoy quality.

To quantify the tFold-TR performance, we adopted a metric Δ GDT-TS to measure the model quality change after refinement. When the TBM decoys of CASP13TBM targets (Figure 4A) are built by CNFPred+RosettaCM pipeline, the refinement performance Δ GDT-TS of tFold-TR (*fixed-delta* strategy) is negatively correlated (Pearson correlation -0.575, p-value < 0.01) with the GDT-TS scores of the initial models. And the performance of *predicted-delta* strategy based tFold-TR shows a higher correlation (Pearson correlation -0.706, p-value < 0.01) with the initial models' qualities. The relationship between tFold-TR performance and initial model qualities is also examined with targets in CAMEO-HY dataset (Figure 4B). The Pearson correlation coefficients are -0.46 and -0.736 for tFold-TR *fixed-delta* strategy and *predicted-delta* strategy respectively.

To summarize, tFold-TR could further improve the qualities of the TBM decoys and the quality improvement performance would be more significant when the initial decoy quality is limited.

3. Discussion

We propose that single-template-based modelling methods have two systematic problems. The first one is that in the template-query alignment, the insertion and missing regions of the query sequence would not receive coordinates information and could not be constraints to maintain short-range and long-range distances. For example, SwissModel⁴⁰ web server would not model the template missing regions of the query sequence in the template-query alignment. Whereas I-TASSER server⁵⁴ uses the ab initio method to model the template missing regions by Replica Exchange Monte simulations⁷⁰. We believe it is necessary to restrict the nearly random modelling of the template missing regions. Therefore, in *fixed-delta* tFold-TR, we implement a distance prediction model to predict inter-residue distances and make a chimeric distance map by filling up the void bins in the TBM decoy derived distance map with the information from the corresponding positions in the predicted distance map.

The other drawback is that for the mutation regions of the template-query alignment, current single-template-based methods consider only unified distance constraint strength for residue pairs. It is commonly known that different amino acids have different mutation rates. And in a template-query alignment, different mutation types thus should have different information contents. For example, if we divide the template-query alignment into different local alignment regions separated by insertion or missing loops (Figure S2), the template-query similarities in these local alignment regions could be diverse. It thus is natural to believe that a more similar local alignment means more reliable local contact interactions from the template in this region. If we extend the idea into a distance map, whether more reliable residue-residue alignment pair would provide a more accurate distance constraint remains to be further explored. Thus, we introduced a simple alignment quality score (AQS) defined by residue mutation scoring matrix BLOSUM62^{71,72} to estimate the reliability of the residue-residue distance constraint extracted from the TBM decoy. The AQSs were incorporated into δ value of the harmonic distance constraints in the 3D modelling by RosettaCM, and the refinement performance is slightly better than *fixed-delta* tFold-TR. Next, we introduced the deviation model (*tFold-RefineNet*) to estimate the quality (distance deviations from ground truth) of the distance map extracted from the TBM initial model. Then in the *predicted-delta* strategy tFold-TR, we provided residue-residue pairwise specific δ value (distance deviations) in the harmonic distance constraints, which further push the modelling accuracy one step forward.

Overall speaking, *fixed-delta* tFold-TR is introduced to tackle the template missing problem while *predicted-delta* tFold-TR directly utilizes the residue-residue pairwise specific δ values to refine the TBM decoys to solve the second problem. In the following sections, we demonstrate the detailed performance gain from these two strategies.

3.1 It is necessary to provide distance constraints for template-missing regions

In the 3D modelling step of a TBM pipeline, the distance map is extracted from the template to serve as stationary distance points in a series of distance constraints. The collection of the distance constraints thus serve as the coarse-grained energy functions to guide gradient-based minimization or Monte Carlo simulations. In both Modeller and RosettaCM, the distance constraints are defined by a harmonic form potential function with two parameters (δ and d_0), where d_0 is the reference stationary distance extracted from template structure and δ works as a constrain strength modulator. A larger δ value therefore would pose a weak distance constraint between a pair of residues' C α atoms (or C β atoms). Since it is not possible to extract coordinates for the missing residues (Figure S2) in the template, whose distances for other residues thus could not be determined either, resulting in deficient qualities for these residues.

It is clear that when the ratio of the missing template residues is high, indicating the target protein is a hard case for modelling, the quality of the TBM decoy tends to be low, and the ratio is indeed negatively correlated (Pearson correlation coefficient -0.588, p-value < 0.01) with initial model quality (GDT-TS score) (Figure 5A). If we feed the modelling process with deep learning predicted distances in the template missing regions, proteins with more missing regions receive large model quality improvement. The quantitative evidence is that the tFold-TR (*fixed-delta* strategy) performance Δ GDT-TS positively correlates (Pearson correlation coefficient 0.656, p-value < 0.01) with the ratio (Figure 5B).

The local modelling qualities (defined by local LDDT scores) of the template missing residues (or called unaligned residues) in the TBM decoys are much lower than other residues (aligned regions and mismatched residues) (Figure 5C, 5D, and Figure S2) in the dataset CASP13TBM. For the TBM (CNFpred+RosettaCM pipeline) decoys, the peak of the local LDDT distribution is around 76.0 for the aligned residues and it is 35.0 for the unaligned

residues. The same goes for the decoys generated by the other two TBM pipelines (HHpred+RosettaCM and BLAST+RosettaCM). The distributions of the local LDDT scores of residues in different regions indicate that the unaligned residues are poorly modelled in single-template-based modelling pipelines. And this evidence also suggests that the modelling qualities of the unaligned residues have a much larger room for improvement.

Then tFold-TR *fixed-delta* strategy is used to refine the TBM decoys, and the distributions of the local LDDT scores of the unaligned residues shift right, indicating that, compared to the initial models, the residues in the unaligned regions in the refined decoys, are better modelled. Meanwhile, the refinement doesn't affect the local qualities of the residues in aligned regions and mismatch regions (Figure 5C and 5D).

Taken target protein T0986s1-D1 as an example (Figure 6), we demonstrate the necessity of providing constraints for the unaligned regions. CNFPred was utilized for template searching and template-query sequence alignment, and 4dsdA was identified as the best template and the overall sequence identity of the alignment is only 8.7%. In the template-query sequence alignment, the N-terminal region of the template is not aligned with the query sequence and this template missing region consists 48.3% of the whole query sequence. While the C-terminal half (residue index 40-93) contains many mismatch residues. It is not surprising that the best template is a very weak one since target T0986s1-D1 is classified as a TBM/FM target. Based on the single-template (4dsdA), the initial model (blue) generated RosettaCM protocol has a GDT-TS=32.9, and its overall folding pattern is quite divergent from the native structure (gray).

tFold-TR (*fixed-delta* strategy) further refined the initial model to a much better 3D model (GDT-TS=75.8), whose overall folding pattern is well aligned with the native structure, with the helices and sheets in the right position and orientation. The Δ LDDT(local) scores, defined by local LDDT scores of the refined model subtracting the scores of the initial TBM model, range from 8 to 62. The residues in the N-terminal half have an average Δ LDDT(local) score around 40.0, while the average Δ LDDT(local) of the C-terminal half of the target protein is less than 30.0. The two peaks (residues 73-79 and 89-93) in the Δ LDDT(local) bar plot coincident with the two beta-sheets. The model from the *predicted-delta* tFold-TR has the highest global quality (GDT-TS=81.2). The local qualities of the N-terminal residues also have been improved, and most of the residues in the C-terminal half have higher Δ LDDT(local) scores than those in the decoy model generated by *fixed-delta* tFold-TR.

All in all, a higher ratio of template missing (unaligned) residues would result in lower quality of the TBM initial model, which could be further refined using tFold-TR by incorporating predicted distances constraints to yield a high-quality 3D model.

3.2 the relationship between alignment quality and modelling accuracy

From the traditional TBM perspective, high-quality template-query alignment is a key input for 3D modelling^{16,17}. However, for a single-template pipeline, current modelling methods do not consider the information that different regions in the alignment would contribute differently to the modelling process, and it is also not clear how to introduce local alignment quality into the modelling.

To further explore the relationship between local alignment quality and local modelling quality, we firstly throw a hypothesis: if two residues are both from highly identical (high quality) alignment regions, then the distance of the two residues (i and j) determined by the corresponding residues in the template structure would also be more reliable, meaning that the distance deviation from the ground true distance in the native structure should be closed to 0), thus the local qualities of residue i and j in the TBM decoy should also be quite high (without considering the short-range and long-range interacting residues). If this hypothesis holds, then

residue i and j should be “trusted” more than other residues, by implementing a stronger constraint (smaller δ value) on the distance between these two residues in the energy function.

To prove that the hypothesis makes sense in some cases, a local alignment quality score (AQS) of residue i (q_i) (Equation 6) is defined by averaging the alignment direct scoring (s_{i-k} to s_{i+k}) based on BLOSUM62 matrix. For example, if the residue i is a Threonine (Thr) and the corresponding residue i in the template is also a Thr, then s_i equals 6. Or residue i in query sequence is a gap open, then -11 is assigned to s_i . Alternatively, if residue i in query sequence is a gap extent, $s_i=-1$. The local alignment quality score of residue i is the average of the direct scoring of the neighbored residues (from residue $i-k$ to $i+k$).

$$q_i = \frac{\sum_{j=i-k}^{i+k} s_j}{2k+1} \quad (6)$$

The statistics support the claim that residues with low AQSs have relatively lower modelling qualities in CASP13TBM and CAMEO-HY datasets. For the targets in these two datasets, CNFpred+RosettaCM pipeline was used for template searching, template-query sequence alignment, and 3D modelling to obtain the best initial models, where both the local AQS scores of the alignment and the local structure quality scores (local LDDT) of the decoys were examined for the mismatched residues.

Clearly, the residues with “good” alignment quality (higher ASQ scores) are naturally modelled by TBM pipeline with “good” structure quality (higher local LDDT scores), and the Pearson Correlation Coefficients are 0.446 (p-value < 0.01) and 0.558 (p-value < 0.01) for CASP13TBM dataset and CAMEO-HY dataset. There is a strong correlation between the local alignment quality and local structure quality, thus it would be reasonable to trust the residues with high local alignment quality during the 3D modelling, and the hypothesis proposed would be partially tested.

To make use of the local alignment quality information in the 3D modelling, especially the δ values in the harmonic constraints, we input the algorithmic average of the AQS of residue i and j into Equation 7 to impact the constraint strengths, however the trial is not very successful since the average GDT-TS scores of the decoys generated by refinement modelling only slightly increased. The problem is we need a direct estimation of δ_{ij} , but we used the average of q_i and q_j , the information may not be direct enough.

Nevertheless, it is still an open question remaining to be further explored. Instead, in this work we are equipped with *tFold-RefineNet* to directly probe the problem, making an estimation of δ_{ij} by predicting the distance deviation (dev_{ij}) between the distance of residue i and j in the decoy and the distance in the native structure, and making use of Equation 6 to transform the dev_{ij} into δ_{ij} . The introduced deviation matrix provides a pairwise-specific δ value prediction thus directly shapes the coarse-grained potential energy function in the 3D modelling.

And tFold-TR improves both local modelling qualities (Figure 7C, 7D, and Figure S2) and global modelling accuracies (Figure 2A-2C). When the residues with low local AQS in the alignment, their local structure qualities (in the initial model) are also low, but after tFold-TR refinement, the local structure quality improvements are more significant. Although the correlation between AQS and Δ LDDT(local) is not very strong for CASP13TBM dataset (-0.184) and CAMEO-HY dataset (-0.415).

Taking T0958-D1 as an example (Figure 8), the initial 3D model of CNFpred+RosettaCM (GDT-TS=38.6) has poor accuracy, the proportion of missing regions in alignment is 11.7%, and the sequence similarity is 13.0%. The accuracy of the 3D structure after optimization by *fixed-delta* strategy reaches 50.0, and the overall modelling accuracy of the second missing

region (31-41) has improved significantly. However, the position of the two β -sheets at the C-terminus of the model is not maintained. In the native structure, there are three β -sheets: residues 20-24, residues 60-65, and residues 71-75. The first and the third should form strand pairing, and this structural pattern is not recovered in both the initial model and the optimized model by *fixed-delta* tFold-TR. And in the model optimized by the *predicted-delta* strategy, the overall accuracy reached 74.7, and the RMSD against the native structure decreases from 12.53 Å to 2.40 Å in the initial model and refined model, while the relative positions of these three β -sheets are closer to the experimental structure, as can be seen in Figure 8, the Δ LDDT(local) scores of the three β -sheet regions in are much higher in *predicted-delta* tFold-TR generated structure.

Another example, T0993s2-D1 (Figure S4), is also from CASP13TBM. the similarity of the alignment of T0993s2-D1 is relatively high and there are no missing regions. The overall accuracy of the 3D structure obtained by CNFpred+RosettaCM for this target is GDT-TS=71.9, and the overall folding is consistent with the experimental structure. After the optimizations by the two strategies of *fixed-delta* and *predicted-delta* by tFold-TR, the accuracy (GDT-TS) of the 3D structure is improved to 76.3 and 81.6.

In summary, we employ pairwise-specific restraints to model the mismatch regions, and this strategy (*predicted-delta*) works better than the *fixed-delta* strategy, partially solving the second drawback of TBM modeling mentioned earlier.

3.3 Continuous improvement of distance deviation prediction is meaningful

We believe that there is room for continued improvement in the structural optimization of the *predicted-delta* strategy. First, with a known native structure, the average accuracy of the initial models from CNFpred+RosettaCM pipeline is GDT-TS=66.0 (CASP13TBM dataset), which can be optimized to 79.8 by the *native-delta* strategy (Supplementary Table). This suggests that our current prediction model for deviations has room for improvement, and by improving the prediction accuracy of deviation, we may be able to continuously improve the performance of *predicted-delta* tFold-TR. Interestingly, we observed a negative correlation between the deviation prediction error RMSE (in Å unit) and the optimization performance of the *predicted-delta* strategy with CASP13TBM dataset (Figure 9). When the RMSE is less than 3 Å, the accuracy of the refined decoy models with multiple targets is greatly improved (Δ GDT-TS > 20). Therefore, it is a potential research direction to continuously improve the prediction accuracy of distance deviation for more accurate template-based decoy refinement.

4. Methods

4.1 Datasets

We collected 3 datasets (from CASP13 and CAMEO platform) to build TBM decoys and refine the with our tFold-TR pipeline.

The first dataset (CASP13TBM) contains all 73 domain-level protein sequences for modelling in CASP13 TBM and TBM/FM categories. The second dataset (CAMEO-3M) contains 74 medium-to-hard proteins collected from CAMEO 3D modelling platform from Sept 2019 to May 2020. The selection criteria are that the $C\alpha$ LDDT score of the decoy predicted by server 999 (single-best-template server) should be less than 40 and the sequence length of a protein should be between 50-300 to avoid too long or too short sequence targets. A third dataset (CAMEO-HY) is also collected from CAMEO, and it is composed by all 182

query sequences used by CAMEO online server predictions during a half-year period (27th Jun. 2020 to 19th Sept. 2020).

For dataset 1, we collected prediction results from Zhang⁴⁶ (group 322) and RaptorX (group 324) from <https://predictioncenter.org/casp13>. As for datasets 2 and 3, we downloaded the predictions from three servers, RaptorX^{42,43}, Robetta⁶⁹, and SwissModel⁴⁰ respectively. All the ground-truth structures of the sequences in the 3 datasets are downloaded from RCSB Protein Data Bank (PDB)⁷³. The target IDs and sequences could be found in the Support Information.

Table 1. The query sequence datasets used to evaluate refinement performance.

SN	Dataset Name	Description	# Sequences	Date Range
1	CASP13TBM	Casp13 TBM and FM/TBM	73	2018.3 to 2018.5
2	CAMEO-HY	Cameo half year hard targets	74	2019.12.7 to 2020.5.30
3	CAMEO-3M	All targets in cameo latest 3 months	182	2020.6.27 to 2020.9.19

4.2 Databases used for MSA searching

For the 3 datasets in Table 1, we used different databases for template searching and MSA searching to feed the distances and deviation prediction deep learning models, as listed in Table 2. The databases are set up here to ensure that there are no data leaks. For example, for both CASP13TBM and CAMEO-HY datasets, we used the databases before the CASP13 competition, while for the CAMEO-3M dataset, we used the November 2019 and earlier versions of the database for all our MSA searching procedures.

Table 2. The databases involved in this paper and the corresponding stamps of them

Database Name	CASP13TBM	CAMEO-HY	CAMEO-3M
Template database	2018.03	2018.03	2019.07
Uniclust30	2017.10	2017.10	2018.08
UniRef90	2018.03	2018.03	2019.07
NR	2018.04	2018.04	2019.11
MetaClust50	2018.01	2018.01	2018.06

4.3 Template searching and TBM decoy generation

tFold-TR takes the predicted inter-residue distance map and inter-residue deviation map, and a TBM generated decoy as inputs, to compose a hybrid potential energy function to build better decoys. For each sequence to be queried, we performed a template search using different threading methods (CNFpred⁷⁴, hhblits v2.0²⁶, and BLAST^{24,25}), and we finally selected the top-ranked one as the single template for modelling. For the CASP13 and CAMEO-HY datasets, their template search was performed against the same template sequence library (PDB non-redundant database before March 2018), while the CAMEO-3M dataset used a somewhat newer template database. The default parameters were used in CNFpred's template search, i.e., a p-value cutoff of 0.005, and *mainScore* was used as the final ranked score. The search parameters for hhblits is e-value 0.001 with 3 iterations, while the other parameters are set as the default values. The template search parameters for BLAST are e-value < 0.01, coverage over 40%.

Ultimately, for the three datasets, the number of targets for which the three different threading methods succeeded in finding the templates varied (Table below), for example, for some hard targets, BLAST and hhblits failed to find useful templates given the searching

parameters. The template-sequence alignments were generated by respective threading methods. Visualization of Alignment was done with the online server AlignmentViewer⁷⁵ (<https://alignmentviewer.org/>).

Table 3. The number of targets for which different threading methods can find templates.

Dataset Name	CNFpred	HHblits	BLAST
CASP13TBM	73	60	34
CAMEO-HY	74	59	49
CAMEO-3M	182	158	135

At the first stage, decoy production is performed according to single-best-template and template-query alignment, both using the standard RosettaCM protocol and Modeller simulation protocol. For each input sequence, each 3D modeling method (RosettaCM or Modeller) produces 300 decoys and the best decoy is selected as input for the next optimization round. In this case, the best decoy generated by RosettaCM is the one with the lowest Rosetta Energy (considering the constraint part). And the best decoy from Modeller is selected by Spicker⁵⁰ to select the center structure of the cluster with the largest population.

4.4 Distance and deviation prediction

The distance prediction is based on a distance prediction model (*tFold-DistNet*) developed by our group, the input features of the model are extracted from Multiple Sequence Alignment (MSA), i.e., Position-Specific Scoring Matrix (PSSM)⁷⁶ and Markov Random Fields (MRF)^{77,78}, through recurrent convolutional layers, it can finally output the inter-residue distances, the inter-residue orientation, as well as backbone dihedral angle and secondary structure prediction. The MSAs were generated by different MSA search tools (hhblits²⁶, HMMER⁷⁹, and BLAST^{24,25}) at different e-values for several databases (Uniclust30, Uniref90, NR, and MetaClust50 as listed in Table 2). Different distance predictions can be obtained by different input MSAs, and the best distance prediction is obtained by clustering and other filtering methods. In addition, we used a 2nd deep learning model (*tFold-RefineNet*) for template decoy inter-residue distance deviation (from the native structure) prediction. The deviation is defined as the absolute difference of the C β atom distance between a pair of residues from the TBM modelled decoy and the native structure. For a query sequence with length L , a TBM pipeline would generate a pool of decoys and select the best decoy (initial model) as the input for the above deviation model, which yields an $L \times L$ deviation matrix. The values in the deviation matrix range from -10\AA to 10\AA . We use the $L \times L$ predicted decoy deviation matrix to determine the strength of the distance constraints for all residue-residue pairs. The two deep learning models would be explained in another paper by our group.

4.5 3D modelling in tFold-TR

For common TBM and FM pipelines, in the 3D modelling phase, they are trying to restrict the distances of all residue pairs as the primary constraints to construct the potential energy equation to find a global minimum. Here, we consider incorporating the distance prediction from *tFold-DistNet* and the TBM decoy, to make a hybrid potential energy function to refine the TBM decoy to generate more accurate 3D models. The following text explains the core idea of how we modify the potential energy functions for TBM decoys refinement.

Based on a threading method for template screening and query-template alignment, and a 3D modeling approach, for any pair of residues (i, j), a constraint g (in Equation 1) is imposed to maintain its distance in a desired range around the distance extracted from template structure.

Generally, for 3D modelling in TBM pipelines (such as RosettaCM), a simple harmonic function (see Equation 2) is used for distance constraints,

$$g(i, j) = \frac{(d_x - d_0)}{\delta} \quad (2)$$

where d_x represents the distance between residue i and j during the modelling, while d_0 is the optimal distance for residue i and j calculated based on template structure. δ is a constant for constraint strength adjustment, a larger δ would enable a weak constraint, and a smaller δ would impose strong restraints for the distance between residue i and j . The essence of the hybrid potential energy function introduced by tFold-TR is the modification of δ and the definition of d_0 : 1) for residue pairs without reliable distance from the template structure, distance model predicts the distances to complete the missing puzzle; 2) for each residue pair, instead of a constant δ , a residue-residue pairwise specific δ is introduced to account for the variable reliabilities of the distances (d_0) extracted from the template structure. Here, in the tFold-TR pipeline, the best decoy from TBM pipeline is used as the *initial structure model* for refinement, which serves as the new “template structure” to extract respective distances between residues.

More specifically, a new equation for constraints is then designed as the following:

$$g(d_{i,j}) = \begin{cases} g_{FM}, & \text{if } align(i, j) = 0 \\ g_{TBM}, & \text{if } align(i, j) = 1 \end{cases} \quad (3)$$

For residues i and j in a TBM decoy, if they both could find aligned counterpart residues in the query-template alignment ($align(i, j)=1$, in the aligned regions of a query-template alignment, Figure S2), their distance reference point d_0 is the distance of the two aligned counterpart residues (C β -C β) in the template (*initial model*). And the distance constraint energy function takes exactly the same formulation as Equation 2, except we used a variable δ_{ij} to replace the original constant δ . The “HARMONIC” type of constraints¹⁷ defined by Rosetta is used to restrict the distance between residue i and j .

However, if either one of residue i or j could not find a counterpart aligned residue in the query-template alignment (in the unaligned regions, Figure S2), we set $align(i, j)$ as 0, and the distance reference d_0 is then taken from the distance map predicted from the distance model. The constraint energy function then is defined as a spline type formed by the logarithm of predicted probabilities of the discrete distances as used by trRosetta. For a spline constraint of the C β -C β , a probability threshold ($p_{cut}=0.2$) is set to determine whether to use this constraint. In addition, all optimization processes used orientations⁴¹ between residues based on deep learning predictions.

To fully evaluate the effects of different δ settings, we adopted 3 strategies for TBM decoy refinement in tFold-TR. For *fixed-delta* tFold-TR, we set δ to 5, which is carefully selected to have the best decoy refinement performance with CASP13TBM dataset. For *predicted-delta* tFold-TR, the constraint energy function adopts a unique $\delta_{i,j}$ for a specific residue pair i and j . Given the TBM decoy, the deviation model predicts a deviation matrix, where each bin contains a predicted inter-residue distance deviation $dev_{i,j}$ between the decoy and the native structure, the $\delta_{i,j}$ is transformed from the absolute value of $dev_{i,j}$ (Equation 5). The third strategy is set to verify where the theoretical upper limit of the modeling accuracy of our optimization algorithm is if the deep learning method can predict the true deviation with 100% accuracy. In this strategy, $dev_{i,j}$ is the absolute value of the difference between the C β atom distance of the residue i and j of the native structure and the decoy.

Table 4. The three strategies deployed with tFold-TR

Strategy Name	δ setting	How δ is determined
<i>fixed-delta</i>	$\delta = 5.0$	A hand-craft parameter

<i>predicted-delta</i>	$\delta_{i,j}$	Deviation model, Equation 4 and 5
<i>native-delta</i>	$\delta_{i,j}$	Deviations between TBM decoy and native structure, Equation 4 and 5

$$g_{TBM}(d_{i,j}) = \left(\frac{d_{i,j}-d_0}{\delta_{i,j}}\right)^2 \quad (4)$$

$$\delta_{i,j} = \begin{cases} 1.0, & \text{if } dev_{i,j} \leq 1.0 \text{ \AA} \\ abs(dev_{i,j}), & \text{if } 1.0 \text{ \AA} < abs(dev_{i,j}) \leq 10.0 \text{ \AA} \\ 10.0, & \text{if } dev_{i,j} > 10.0 \text{ \AA} \end{cases} \quad (5)$$

tFold-TR's structural optimization starts with the best decoys obtained from RosettaCM or Modeller. The optimization protocol is based on PyRosetta: inputting a TBM decoy as the initial model, starting with multiple rounds of energy minimization in centroid mode, followed by a full-atom fast-relax, and then clash removal. For one TBM initial decoy, 50 decoys are generated from tFold-TR protocols, and the decoy with the lowest energy (Rosetta energy + constraint energy) is then selected as the final refinement result.

4.6 Evaluation metrics

In the TBM step, and the later structural refinement using tFold-TR, only one decoy (with the best energy) was selected for the performance analysis.

We use different metrics for decoy quality evaluation. Taking a decoy as a whole, we evaluate the similarity between the decoy and the native structure by TMscore⁸⁰, LDDT (global)⁸¹, and GDT-TS⁸². We used DeepScore⁸³ to calculate GDT-TS and TMscore, and our in-house LDDT_Assess tool to perform global and local LDDT calculations. In this paper, unless otherwise stated, LDDT refers to the LDDT (global) and is an overall quality score of the decoy, while local LDDT is a local quality assessment at the residue level. The ranges of both TMscore, LDDT, GDT-TS, and local LDDT are ranging from 0 to 100. A higher score indicates a better global or local quality of the decoy.

Reference

1. Agarwal, B. K. X-Ray Spectroscopy, An Introduction. *J. Opt.* (1979)
doi:10.1007/bf03549011.
2. Smyth, M. S. & Martin, J. H. J. x Ray crystallography. *Journal of Clinical Pathology - Molecular Pathology* (2000) doi:10.1136/mp.53.1.8.
3. Atkinson, R. A. NMR of proteins and nucleic acids. *Nucl. Magn. Reson.* (2021)
doi:10.1039/9781788010665-00250.
4. Simpson, P. J. NMR of proteins and nucleic acids. *Nuclear Magnetic Resonance* (2015) doi:10.1039/9781782622758-00348.

5. Wüthrich, K. NMR with Proteins and Nucleic Acids. *Europhys. News* (1986)
doi:10.1051/eprn/19861701011.
6. Chu, B. & Hsiao, B. S. Small-angle X-ray scattering of polymers. *Chemical Reviews*
(2001) doi:10.1021/cr9900376.
7. Feigin, L. A. & Svergun, D. I. *Structure Analysis by Small-Angle X-Ray and Neutron Scattering*. *Structure Analysis by Small-Angle X-Ray and Neutron Scattering* (1987).
doi:10.1007/978-1-4757-6624-0.
8. Bóta, A. Biological small angle scattering. *Crystallogr. Rev.* (2019)
doi:10.1080/0889311x.2019.1592168.
9. Savva, C. A beginner's guide to cryogenic electron microscopy. *Biochem. (Lond)*.
(2019) doi:10.1042/bio04102046.
10. Elmlund, D. & Elmlund, H. Cryogenic electron microscopy and single-particle analysis. *Annual Review of Biochemistry* (2015) doi:10.1146/annurev-biochem-060614-034226.
11. Adrian, M., Dubochet, J., Lepault, J. & McDowell, A. W. Cryo-electron microscopy of viruses. *Nature* (1984) doi:10.1038/308032a0.
12. Dubach, V. R. A. & Guskov, A. The resolution in x-ray crystallography and single-particle cryogenic electron microscopy. *Crystals* (2020) doi:10.3390/cryst10070580.
13. Kuhlman, B. & Baker, D. Native protein sequences are close to optimal for their structures. *Proc. Natl. Acad. Sci. U. S. A.* (2000) doi:10.1073/pnas.97.19.10383.
14. Vella, F. Introduction to Protein Structure. *Biochem. Educ.* (1992) doi:10.1016/0307-4412(92)90132-6.
15. Rangwala, H. & Karypis, G. Introduction to Protein Structure Prediction. in *Introduction to Protein Structure Prediction: Methods and Algorithms* (2010).
doi:10.1002/9780470882207.ch1.

16. Webb, B. & Sali, A. Comparative protein structure modeling using MODELLER. *Curr. Protoc. Bioinforma.* (2016) doi:10.1002/cpbi.3.
17. Song, Y. *et al.* High-resolution comparative modeling with RosettaCM. *Structure* (2013) doi:10.1016/j.str.2013.08.005.
18. Fiser, A. Template-based protein structure modeling. *Methods in molecular biology (Clifton, N.J.)* (2010) doi:10.1007/978-1-60761-842-3_6.
19. Kopp, J., Bordoli, L., Battey, J. N. D., Kiefer, F. & Schwede, T. Assessment of CASP7 predictions for template-based modeling targets. in *Proteins: Structure, Function and Genetics* (2007). doi:10.1002/prot.21753.
20. Gembarski, P. C., Li, H. & Lachmayer, R. Template-based modelling of structural components. *Int. J. Mech. Eng. Robot. Res.* (2017) doi:10.18178/ijmerr.6.5.336-342.
21. Zhang, Y. Template-based modeling and free modeling by I-TASSER in CASP7. in *Proteins: Structure, Function and Genetics* (2007). doi:10.1002/prot.21702.
22. Venclovas, Č. & Margelevičius, M. The use of automatic tools and human expertise in template-based modeling of CASP8 target proteins. *Proteins Struct. Funct. Bioinforma.* (2009) doi:10.1002/prot.22515.
23. Croll, T. I., Sammito, M. D., Kryshchuk, A. & Read, R. J. Evaluation of template-based modeling in CASP13. *Proteins Struct. Funct. Bioinforma.* (2019) doi:10.1002/prot.25800.
24. Camacho, C. *et al.* BLAST+: Architecture and applications. *BMC Bioinformatics* (2009) doi:10.1186/1471-2105-10-421.
25. McGinnis, S. & Madden, T. L. BLAST: At the core of a powerful and diverse set of sequence analysis tools. *Nucleic Acids Res.* (2004) doi:10.1093/nar/gkh435.
26. Remmert, M., Biegert, A., Hauser, A. & Söding, J. HH-suite for sensitive sequence searching based on HMM-HMM alignment. *Nat. Methods* (2011).

27. Sasai, M. Conformation, energy, and folding ability of selected amino acid sequences. *Proc. Natl. Acad. Sci. U. S. A.* (1995) doi:10.1073/pnas.92.18.8438.
28. Levitt, M. Protein folding by restrained energy minimization and molecular dynamics. *J. Mol. Biol.* (1983) doi:10.1016/S0022-2836(83)80129-6.
29. Church, B. W. & Shalloway, D. Top-down free-energy minimization on protein potential energy landscapes. *Proc. Natl. Acad. Sci. U. S. A.* (2001) doi:10.1073/pnas.101030498.
30. De Sancho, D. & Rey, A. Energy minimizations with a combination of two knowledge-based potentials for protein folding. *J. Comput. Chem.* (2008) doi:10.1002/jcc.20924.
31. Zheng, L., Alhossary, A. A., Kwok, C. K. & Mu, Y. Molecular dynamics and simulation. in *Encyclopedia of Bioinformatics and Computational Biology: ABC of Bioinformatics* (2018). doi:10.1016/B978-0-12-809633-8.20284-7.
32. Karplus, M. & Petsko, G. A. Molecular dynamics simulations in biology. *Nature* (1990) doi:10.1038/347631a0.
33. Shen, M. & Sali, A. Statistical potential for assessment and prediction of protein structures. *Protein Sci.* (2006) doi:10.1110/ps.062416606.
34. Alford, R. F. *et al.* The Rosetta All-Atom Energy Function for Macromolecular Modeling and Design. *J. Chem. Theory Comput.* (2017) doi:10.1021/acs.jctc.7b00125.
35. Allinger, N. L., Zhou, X. & Bergsma, J. Molecular mechanics parameters. *J. Mol. Struct. THEOCHEM* (1994) doi:10.1016/S0166-1280(09)80008-0.
36. Molecular mechanics across chemistry. *Choice Rev. Online* (1997) doi:10.5860/choice.35-0914.
37. Pastor, R. W. & MacKerell, A. D. Development of the CHARMM force field for lipids. *Journal of Physical Chemistry Letters* (2011) doi:10.1021/jz200167q.

38. Zhu, X., Lopes, P. E. M. & Mackerell, A. D. Recent developments and applications of the CHARMM force fields. *Wiley Interdisciplinary Reviews: Computational Molecular Science* (2012) doi:10.1002/wcms.74.
39. Eswar, N. *et al.* Comparative Protein Structure Modeling Using MODELLER. *Curr. Protoc. Protein Sci.* (2007) doi:10.1002/0471140864.ps0209s50.
40. Biasini, M. *et al.* SWISS-MODEL: Modelling protein tertiary and quaternary structure using evolutionary information. *Nucleic Acids Res.* (2014) doi:10.1093/nar/gku340.
41. Yang, J. *et al.* trRosetta. *Proc. Natl. Acad. Sci. U. S. A.* (2020) doi:10.1073/pnas.1914677117.
42. Xu, J. Distance-based protein folding powered by deep learning. *Proc. Natl. Acad. Sci. U. S. A.* (2019) doi:10.1073/pnas.1821309116.
43. Wang, S., Sun, S., Li, Z., Zhang, R. & Xu, J. Accurate De Novo Prediction of Protein Contact Map by Ultra-Deep Learning Model. *PLoS Comput. Biol.* (2017) doi:10.1371/journal.pcbi.1005324.
44. Adhikari, B. & Cheng, J. CONFOLD2: Improved contact-driven ab initio protein structure modeling. *BMC Bioinformatics* (2018) doi:10.1186/s12859-018-2032-6.
45. Adhikari, B., Bhattacharya, D., Cao, R. & Cheng, J. CONFOLD: Residue-residue contact-guided ab initio protein folding. *Proteins Struct. Funct. Bioinforma.* (2015) doi:10.1002/prot.24829.
46. Zheng, W. *et al.* Deep-learning contact-map guided protein structure prediction in CASP13. *Proteins Struct. Funct. Bioinforma.* (2019) doi:10.1002/prot.25792.
47. Hou, J., Wu, T., Guo, Z., Quadri, F. & Cheng, J. The MULTICOM Protein Structure Prediction Server Empowered by Deep Learning and Contact Distance Prediction. in *Methods in Molecular Biology* (2020). doi:10.1007/978-1-0716-0708-4_2.
48. Benkert, P., Tosatto, S. C. E. & Schwede, T. Global and local model quality estimation

- at CASP8 using the scoring functions QMEAN and QMEANclust. *Proteins Struct. Funct. Bioinforma.* (2009) doi:10.1002/prot.22532.
49. Zhou, H. & Skolnick, J. GOAP: A generalized orientation-dependent, all-atom statistical potential for protein structure prediction. *Biophys. J.* (2011) doi:10.1016/j.bpj.2011.09.012.
 50. Zhang, Y. & Skolnick, J. SPICKER: A clustering approach to identify near-native protein folds. *J. Comput. Chem.* (2004) doi:10.1002/jcc.20011.
 51. Hancock, J. M., Zvelebil, M. J. & Dunbrack, R. SwissModel. in *Dictionary of Bioinformatics and Computational Biology* (2004). doi:10.1002/9780471650126.dob0720.pub2.
 52. Zhang, Y. I-TASSER server for protein 3D structure prediction. *BMC Bioinformatics* (2008) doi:10.1186/1471-2105-9-40.
 53. Yang, J. *et al.* The I-TASSER suite: Protein structure and function prediction. *Nature Methods* (2014) doi:10.1038/nmeth.3213.
 54. Roy, A., Kucukural, A. & Zhang, Y. I-TASSER: A unified platform for automated protein structure and function prediction. *Nat. Protoc.* (2010) doi:10.1038/nprot.2010.5.
 55. Zhang, Y. I-TASSER: Fully automated protein structure prediction in CASP8. *Proteins Struct. Funct. Bioinforma.* (2009) doi:10.1002/prot.22588.
 56. Källberg, M. *et al.* Template-based protein structure modeling using the RaptorX web server. *Nat. Protoc.* (2012) doi:10.1038/nprot.2012.085.
 57. Morten, K. *et al.* Template-based Protein Structure Modelling using the RaptorX web server. *Nat. Protoc.* (2012).
 58. Peng, J. & Xu, J. Raptorx: Exploiting structure information for protein alignment by statistical inference. *Proteins Struct. Funct. Bioinforma.* (2011)

- doi:10.1002/prot.23175.
59. Senior, A. W. *et al.* Improved protein structure prediction using potentials from deep learning. *Nature* (2020) doi:10.1038/s41586-019-1923-7.
 60. Alquraishi, M. AlphaFold at CASP13. *Bioinformatics* (2019) doi:10.1093/bioinformatics/btz422.
 61. López-Blanco, J. R. & Chacón, P. KORP: Knowledge-based 6D potential for fast protein and loop modeling. *Bioinformatics* (2019) doi:10.1093/bioinformatics/btz026.
 62. Peng, H. P. & Yang, A. S. Modeling protein loops with knowledge-based prediction of sequence-structure alignment. *Bioinformatics* (2007) doi:10.1093/bioinformatics/btm456.
 63. Webb, B. & Sali, A. Protein structure modeling with MODELLER. in *Methods in Molecular Biology* (2017). doi:10.1007/978-1-4939-7231-9_4.
 64. Buenavista, M. T., Roche, D. B. & McGuffin, L. J. Improvement of 3D protein models using multiple templates guided by single-template model quality assessment. *Bioinformatics* (2012) doi:10.1093/bioinformatics/bts292.
 65. Larsson, P., Skwark, M. J., Wallner, B. & Elofsson, A. Improved predictions by Pcons.net using multiple templates. *Bioinformatics* (2011) doi:10.1093/bioinformatics/btq664.
 66. Chakravarty, S., Godbole, S., Zhang, B., Berger, S. & Sanchez, R. Systematic analysis of the effect of multiple templates on the accuracy of comparative models of protein structure. *BMC Struct. Biol.* (2008) doi:10.1186/1472-6807-8-31.
 67. Zheng, W. *et al.* Detecting distant-homology protein structures by aligning deep neural-network based contact maps. *PLoS Comput. Biol.* (2019) doi:10.1371/journal.pcbi.1007411.
 68. Li, Y. *et al.* Deducing high-accuracy protein contact-maps from a triplet of

- coevolutionary matrices through deep residual convolutional networks. *PLOS Comput. Biol.* (2021) doi:10.1371/journal.pcbi.1008865.
69. Leman, J. K. *et al.* Macromolecular modeling and design in Rosetta: recent methods and frameworks. *Nature Methods* (2020) doi:10.1038/s41592-020-0848-2.
 70. Okabe, T., Kawata, M., Okamoto, Y. & Mikami, M. Replica-exchange Monte Carlo method for the isobaric-isothermal ensemble. *Chem. Phys. Lett.* (2001) doi:10.1016/S0009-2614(01)00055-0.
 71. Rédei, G. P. BLOSUMS. in *Encyclopedia of Genetics, Genomics, Proteomics and Informatics* (2008). doi:10.1007/978-1-4020-6754-9_1926.
 72. Eddy, S. R. Where did the BLOSUM62 alignment score matrix come from? *Nature Biotechnology* (2004) doi:10.1038/nbt0804-1035.
 73. Berman, H. M. *et al.* The Protein Data Bank. *Nucleic Acids Research* (2000) doi:10.1093/nar/28.1.235.
 74. Zhu, J., Wang, S., Bu, D. & Xu, J. Protein threading using residue co-variation and deep learning. in *Bioinformatics* (2018). doi:10.1093/bioinformatics/bty278.
 75. Sander, C. *et al.* AlignmentViewer: Sequence Analysis of Large Protein Families. *F1000Research* (2020) doi:10.12688/f1000research.22242.2.
 76. Jones, D. T. Protein secondary structure prediction based on position-specific scoring matrices. *J. Mol. Biol.* (1999) doi:10.1006/jmbi.1999.3091.
 77. Kindermann, R. & Snell, J. L. Markov random fields and their applications. *Science* (1980).
 78. White, J. V., Muchnik, I. & Smith, T. F. Modeling protein cores with Markov random fields. *Math. Biosci.* (1994) doi:10.1016/0025-5564(94)90041-8.
 79. Hancock, J. M. & Bishop, M. J. HMMer. in *Dictionary of Bioinformatics and Computational Biology* (2004). doi:10.1002/9780471650126.dob0323.pub2.

80. Zhang, Y. & Skolnick, J. TM-align: A protein structure alignment algorithm based on the TM-score. *Nucleic Acids Res.* (2005) doi:10.1093/nar/gki524.
81. Mariani, V., Biasini, M., Barbato, A. & Schwede, T. IDDT: A local superposition-free score for comparing protein structures and models using distance difference tests. *Bioinformatics* (2013) doi:10.1093/bioinformatics/btt473.
82. Zemla, A., Venclovas, Č., Reinhardt, A., Fidelis, K. & Hubbard, T. J. Numerical criteria for the evaluation of ab initio predictions of protein structure. *Proteins Struct. Funct. Genet.* (1997) doi:10.1002/(SICI)1097-0134(1997)1+<140::AID-PROT19>3.0.CO;2-O.
83. Wang, S., Ma, J., Peng, J. & Xu, J. Protein structure alignment beyond spatial proximity. *Sci. Rep.* (2013) doi:10.1038/srep01448.

Figure Captions

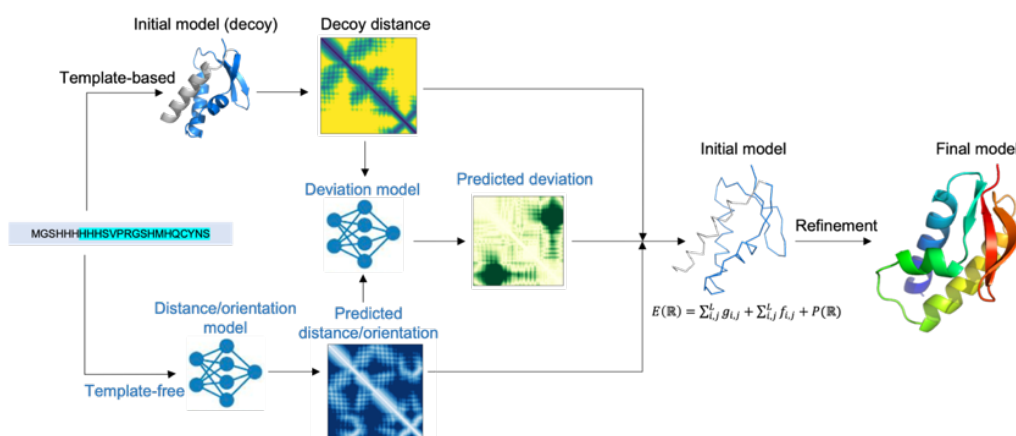


Figure 1. the tFold-TR pipeline. The query sequence is firstly modelled by a TBM method to obtain the best template-based decoy (initial decoy). Next, through the distance model (*tFold-DistNet*), the distance map for the query sequence is predicted. By providing the decoy distance map and the predicted distance map, another deviation model (*tFold-RefineNet*) predicts the distance deviation matrix for the initial decoy. Combining the decoy distance map, predicted distance map, and the deviation map, a hybrid potential energy function is derived to guide the structure refinement of the initial decoy structure.

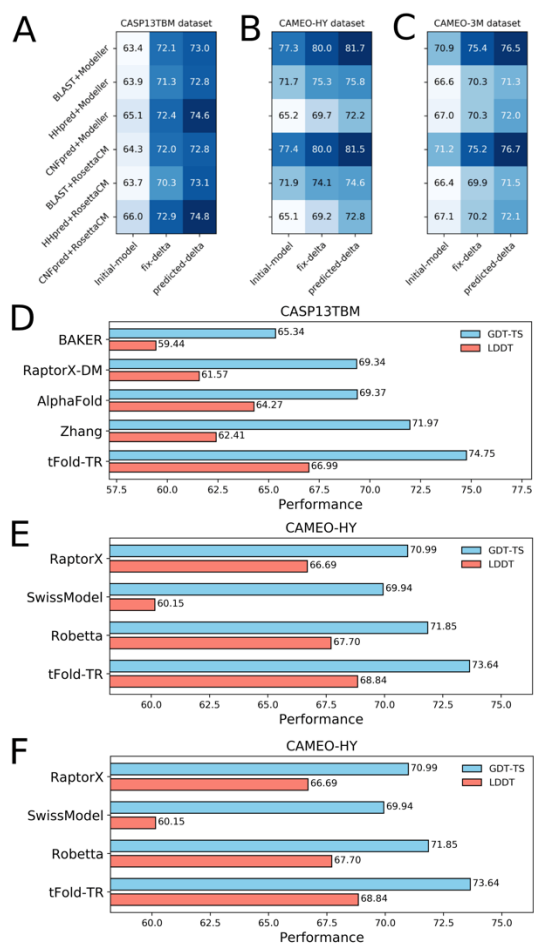


Figure 2. The performance of the hybrid potential-based approach tFold-TR for structural optimization. A-C, each bin gets a value indicating the average GDT-TS, and the darker the bin, the higher the average GDT-TS. D-E, the performance of different folding algorithms (servers) on the three datasets, where blue indicates GDT-TS and red indicates LDDT. Note that RaptorX-DM in panel D refers to RaptorX-DeepModeller, and in E, RaptorX, SwissModel, and Robetta submitted a common set of 72 (out of 74) targets, where the performance of all methods is therefore averaged over the 72 targets. On the CAMEO-3M dataset in panel E, RaptorX skipped 88 targets, while SwissModel and Robetta have fewer missing decoys, so the performance of RaptorX is represented by the average score of the submitted 94 targets, while for SwissModel, Robetta, and tFold-TR, the performance is evaluated with the common 171 targets.

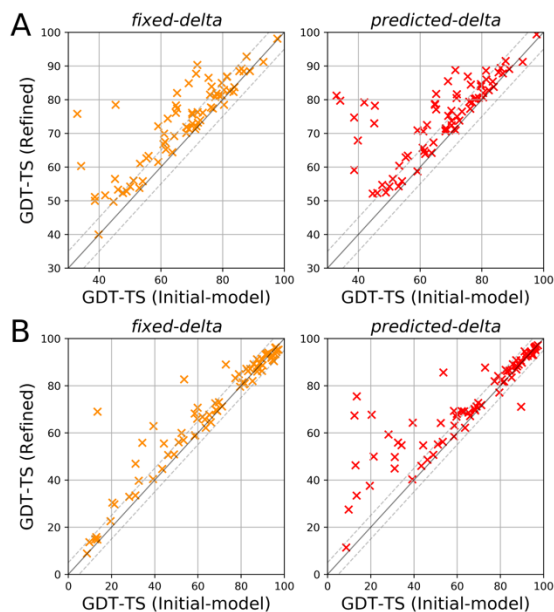


Figure 3. The performance of tFold-TR refinement of initial models for CASP13TBM dataset (A) and CAMEO-3M dataset (B). The initial models (TBM decoys) were built by RosettaCM. The gray dashed lines indicate ± 5 GDT-TS range.

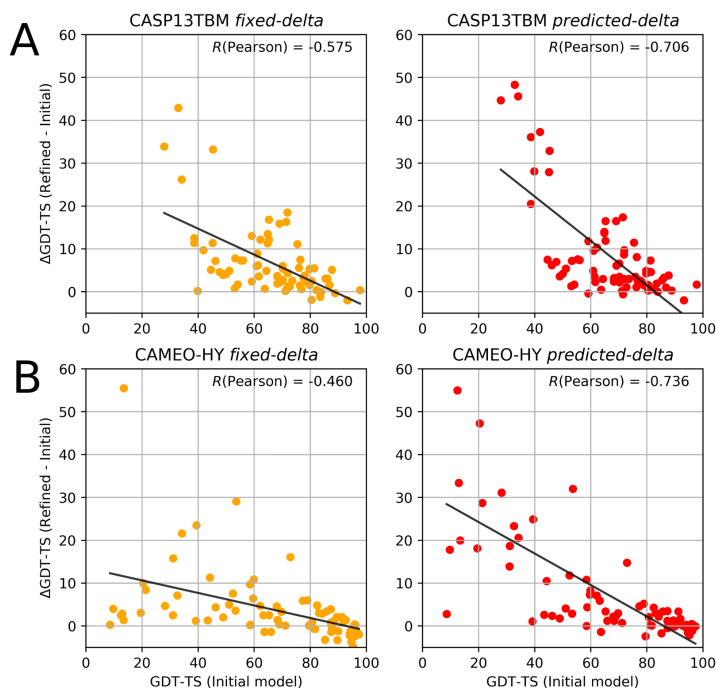


Figure 4. The effect of structural optimization is negatively correlated with the model accuracy of the initial TBM decoys for CASP13TBM dataset (A) and CAMEO-HY dataset (B).

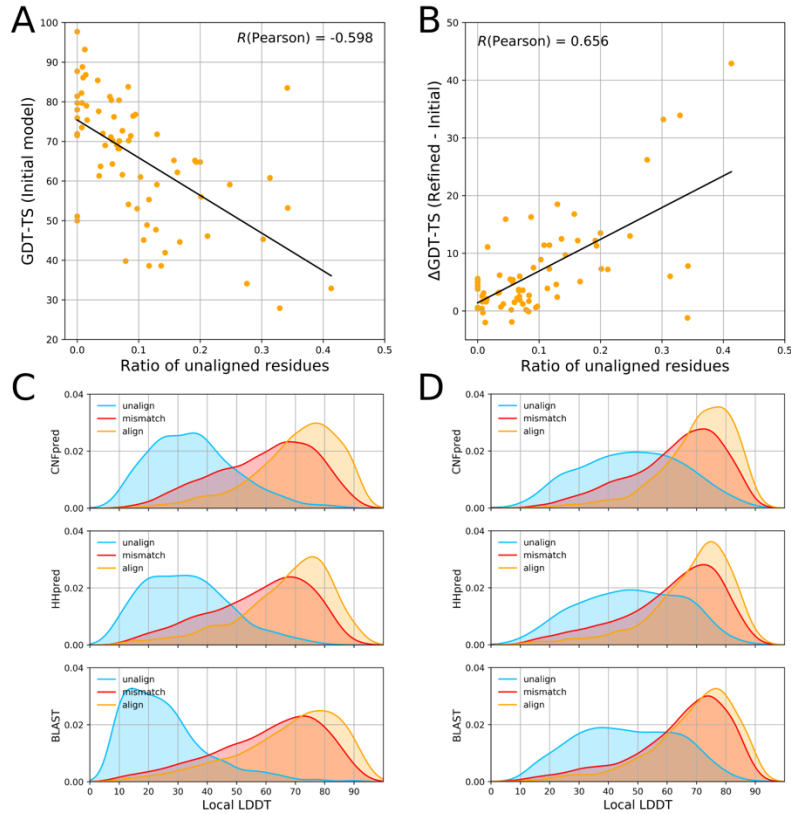


Figure 5. The proportion of unaligned regions in template-query alignment in the CASP13TBM dataset is related to the accuracy of the TBM modeling and the structural optimization by tFold-TR. A, the relationship between the ratio of unaligned in GDT-TS and alignment of the initial model obtained by CNFpred+RosettaCM. B, the relationship between the ratio of unaligned residues in GDT-TS and alignment after *fixed-delta* tFold-TR optimization. C, the distribution of local LDDT in different regions of the alignment of the initial model obtained by CNFpred+RosettaCM. D, local LDDT distribution of different regions of the alignment after *fixed-delta* tFold-TR refinement.

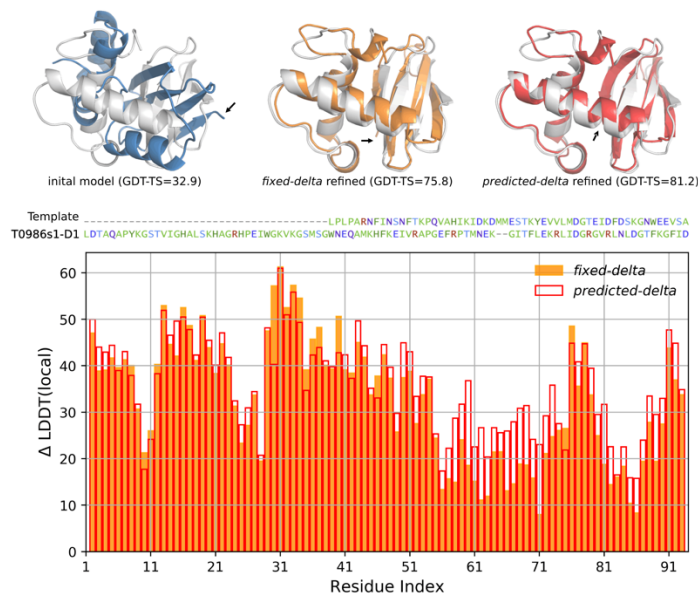


Figure 6. The refinement performance of tFold-TR for target T0986s1-D1. The native structure of T0986s1-D1 is shown as gray color in the top panels. The black arrows in the top panels indicate the C-terminal region of the domain.

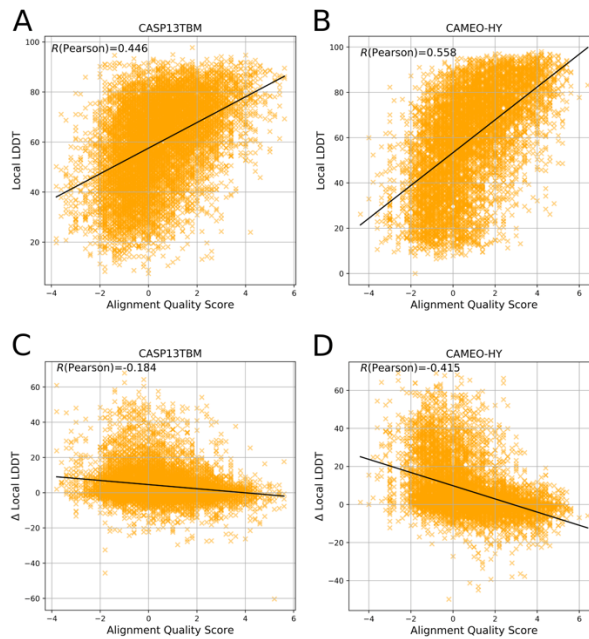


Figure 7. The relationship between the AQS of amino acids and initial model local LDDT and the accuracy improvement after structure optimization. A and C, based on CASP13TBM dataset, initial model from CNFpred+RosettaCM. B and D, based on CAMEO-HF dataset, initial model from CNFpred+RosettaCM.

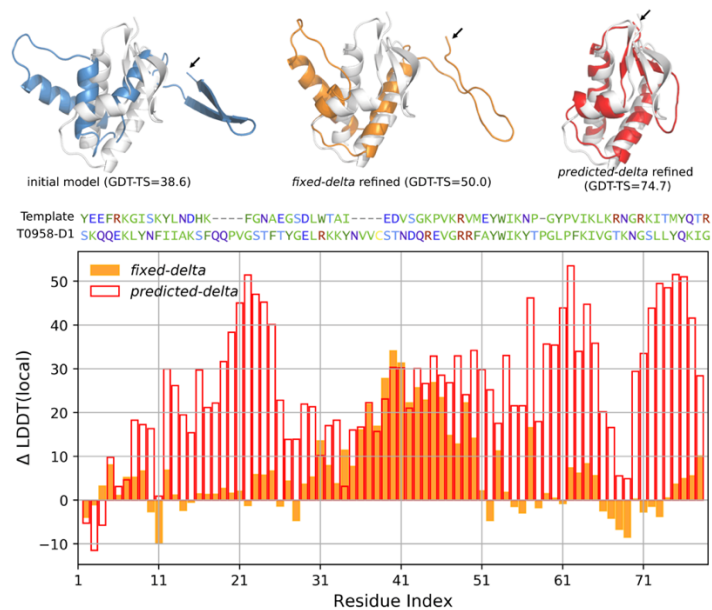


Figure 8. The refinement performance of tFold-TR for target T0958-D1. The native structure of T0985-D1 is shown as gray color in the top panels. The black arrows in the top panels indicate the C-terminal region of the domain.

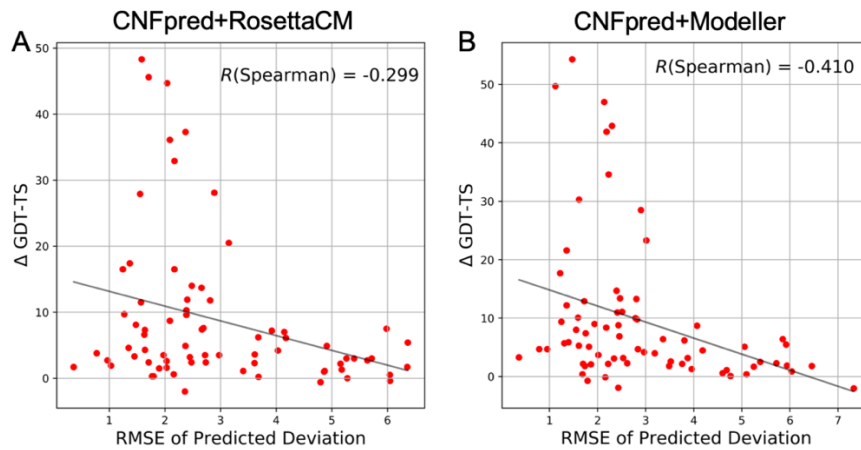


Figure 9. Relationship between distance deviation prediction error with refinement (*predicted-delta* strategy) performance. The evaluations are calculated on CASP13TBM dataset for initial models. Δ GDT-TS is defined as GDT-TS (*predicted-delta* refined) - GDT-TS (initial model). A, the refinement is conducted with CNFpred+RosettaCM initial models. B, the refinement is conducted with CNFpred+Modeller initial models.

Support Information Captions

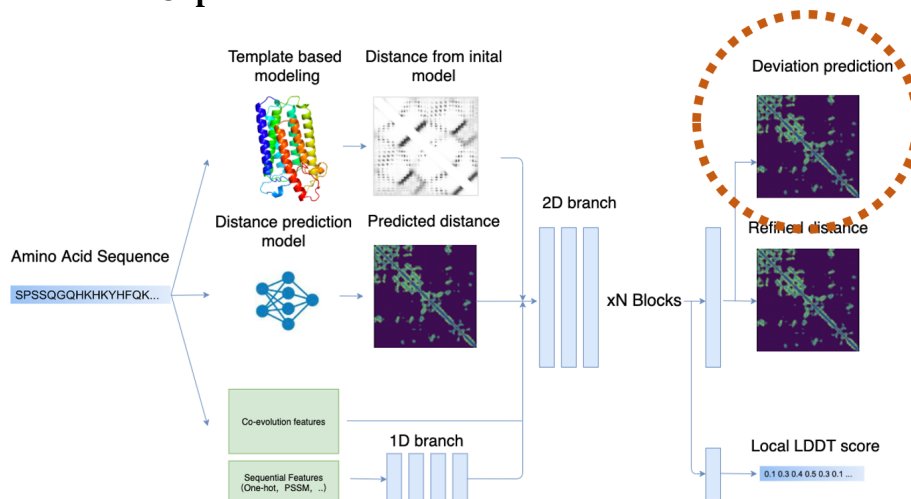


Figure S1. Deviation prediction deep learning model (*tFold-RefineNet*) pipeline.

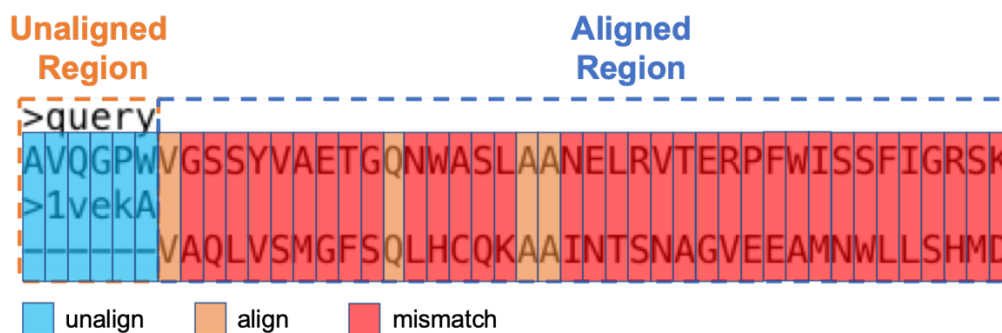


Figure S2. The different types of query-template alignment residues.

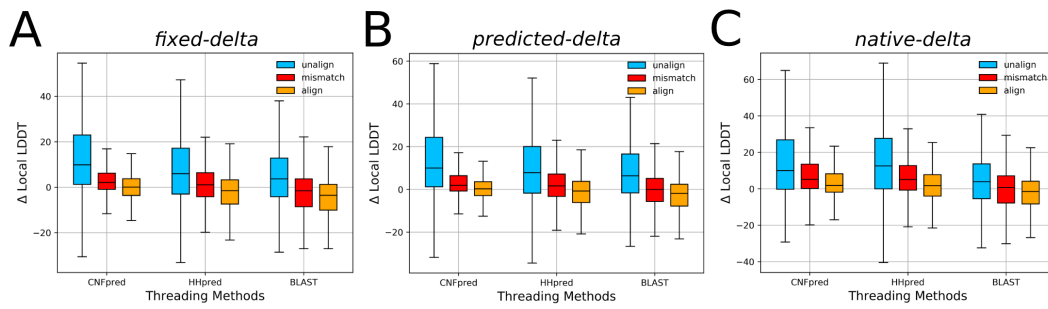


Figure S3. The accuracy increase of decoys generated RosettaCM TBM pipelines in 3 alignment regions brought by tFold-TR with three strategies on CASP13TBM dataset.

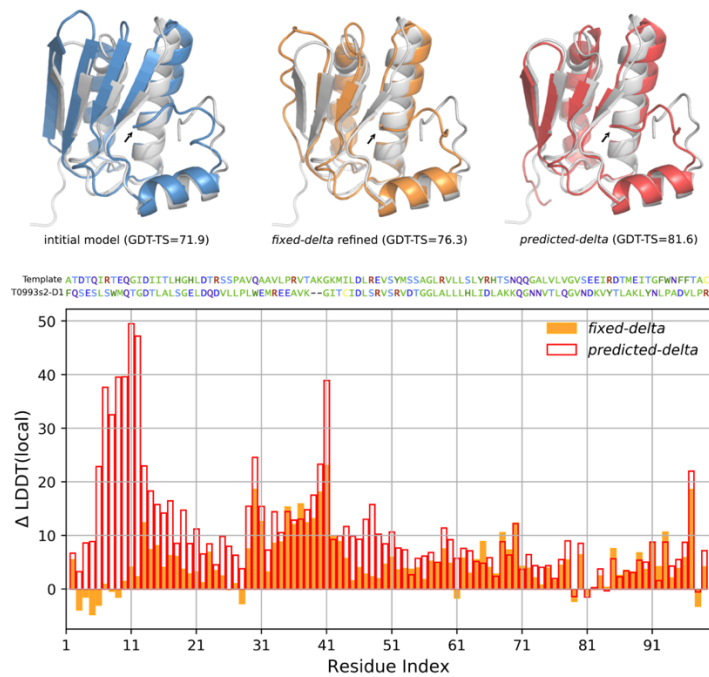


Figure S4. Structure comparison and local LDDT enhancement for T0993s2-D1 structure optimization.